# City Research Online

## City, University of London Institutional Repository

This is the accepted version of the paper.

This version of the publication may differ from the final published version.

# Risk-informed optimization of the tuned mass-damper-inerter (TMDI) for the seismic protection of multi-storey building structures

R. Ruiz[(1)], A.A Taflanidis[(2)], A. Giaralis[(3)] and D. Lopez-Garcia[(4)]

[1]*Department of Civil Engineering, Universidad de Chile*
[2]*Department of Civil & Environmental Engineering & Earth Sciences, University of Notre Dame*
[3] *Department of Civil Engineering, City University of London*
[4] *Department of Structural and Geotechnical Engineering, Pontificia Universidad Católica de Chile & National Research Center for Integrated Natural Disaster Management CONICYT FONDAP 15110017*

## Abstract

The tuned mass-damper-inerter (TMDI) is a recently proposed passive vibration suppression device that couples the classical tuned mass-damper (TMD), comprising a secondary mass attached to the structure via a spring and dashpot, with an inerter. The latter is a two-terminal mechanical device developing a resisting force proportional to the relative acceleration of its terminals by the "inertance" constant. In a number of previous studies, optimally tuned TMDIs have been shown to outperform TMDs in mitigating earthquake-induced vibrations in building structures for the same pre-specified secondary mass. TMDI design in these studies involved simplified modeling assumptions, such as adopting a single performance objective and/or modeling seismic excitation as stationary stochastic process. This paper extends these efforts by examining a risk-informed TMDI optimization, adopting multiple objectives and using response history analysis and probabilistic life-cycle criteria to quantify performance. The first performance criterion, representing overall direct benefits, is the life-cycle cost of the system, composed of the upfront TMDI cost and the anticipated seismic losses over the lifetime of the structure. The second performance criterion, introducing risk-aversion attitudes into the design process, is the repair cost with a specific return period (i.e., probability of exceedance over the lifetime of the structure). The third performance criterion, accounting for practical constraints associated with the size of the inerter and its connection to the structure, is the inerter force with a specific return period. A particular variant of the design problem is also examined by combining the first and third performance criteria/objectives. A case study involving a 21-storey building constructed in Santiago, Chile shows that optimal TMDI configurations can accomplish simultaneous reduction of life-cycle and repair costs. However, these cost reductions come at the expense of increased inerter forces. It is further shown that connecting the inerter to lower floors provides considerable benefits across all examined performance criteria as the inerter is engaged in a more efficient way for the same inerter coefficient and attached mass ratios.

**Keywords:** tuned mass damper inerter; life-cycle analysis; risk-informed optimal design; cost-based optimization

## 1. Introduction

Inertia/mass dampers, with most popular representative the tuned mass-damper (TMD), have been extensively used for passive vibration suppression of dynamically excited multi-storey buildings [1-4]. They consist of an inertial vibrating element (secondary mass) attached to a higher floor of the primary/host building structure to be controlled. Through appropriate tuning of its vibratory characteristics, the secondary mass counteracts the motion of the host structure enabling kinetic energy dissipation [5]. For the classical TMD, this is achieved through connection of the secondary mass by optimally tuned linear spring and viscous damper (dashpot) elements. The effectiveness of mass dampers depends heavily on their inertia property, i.e. the size of the secondary mass which, in conventional tuning approaches, is *a priori* set. This is particularly true for seismic applications which require large secondary TMD mass for efficient vibration suppression [6-9] due to the transient and non-stationary characteristics of earthquake-induced ground motion excitation. Nevertheless, large secondary mass increases the cost of TMD implementation as well as the additional gravity loads to be accommodated by the primary structure. This has incentivized a number of researchers [10-12] to propose optimal TMD design approaches which treat the TMD mass as design variable. Given that seismic performance is monotonically improved with increasing TMD mass, one way to rationally incorporate the attached mass in the TMD design problem considers using life-cycle cost criteria [11, 12]: an approach widely used to evaluate benefits offered by various supplemental damping devices [13-15]. Conveniently, this approach facilitates a comprehensive evaluation of performance using metrics that are relevant to the stakeholders of a building, such as repair and/or total cost leading to performance-based TMD design beyond standard TMD tuning for heuristically pre-specified secondary mass.

For tackling practical constraints related to the size of the secondary mass and further improving performance of mass dampers for the seismic protection of building structures, a generalization of the classical TMD was proposed by the third author [16, 17], incorporating an inerter element: the tuned mass-damper-inerter (TMDI). The inerter is a two-terminal mechanical element developing a resisting force proportional to the relative acceleration of its terminals, with proportionality constant expressed in mass (kg) units and termed "inertance" [18]. Supplemental damping devices for seismic applications incorporating inerters with inertance several orders of magnitude larger than the physical device mass have been prototyped and experimentally verified in recent years [19, 20]. In this respect, in the TMDI configuration, the inerter, taken as an ideal massless mechanical element, increases through its inertance the apparent inertial property of the TMD for a given secondary mass without increasing its weight. This is achieved by connecting the TMD mass via the inerter to a *different* floor from the one that the TMD is attached to in a multi-storey primary building structure as depicted in Figure 1. This configuration influences the dynamic response of the primary structure in a wide frequency range and not only at frequencies close to the own mass damper oscillation frequency, as is the case of the classical TMD [21, 22]. Notably, a number of other inerter-based mass dampers and supplemental damping devices have been proposed in the literature for the seismic

Ruiz R, Taflanidis AA, **Giaralis A,** Lopez-Garcia D. (2018). Risk-informed optimization of the tuned mass-damper-inerter (TMDI) for the seismic protection of multi-storey building structures**.** *Engineering Structures,* **177**: 836-850.

protection of building structures, including the tuned viscous-mass-damper [23], the tuned inerter-damper [24], and the rotational inertia damper [25]. Whilst the TMDI is exclusively treated herein, the theoretical framework for probabilistic performance design and assessment discussed in this paper is applicable to any of the above passive control device configurations incorporating inerters.

In a number of seismic application studies [17, 22, 26, 27], the TMDI was shown to outperform the TMD, especially for relatively small secondary attached mass. Further, an important aspect in the TMDI design is the impact of the inerter topological configuration on the performance of TMDI-equipped structures; it was shown by Giaralis and Taflanidis [22] that TMDI configurations with the inerter linking the secondary mass to a lower floor than the floor immediately underneath the mass damper provide significantly enhanced performance (see also [28]). Nevertheless, all previous TMDI seismic application studies considered shear type building frame structures, while optimal TMDI tuning was undertaken for seismic excitations represented by stationary stochastic processes. More importantly, neither the TMDI cost nor the inerter force exerted on the host structure were explicitly considered in the TMDI design. In fact, such simplified structural and seismic excitation modeling, as well as performance evaluation settings, extend to all relevant studies that addressed the optimal seismic design of different types of inerter-based mass dampers and supplement damping devices such as the tuned viscous-mass-damper [29], the tuned inerter-damper [30-32], and rotational inertia dampers [33].



$$F_b = b(\ddot{y} - \ddot{x}_{i_b}), \quad b = m_f \frac{\gamma_f^2}{\gamma_{pr}^2} \left[ \prod_{k=1}^{n} \frac{r_k^2}{pr_k^2} \right]$$

Figure 1.  Tuned mass-damper-inerter (TMDI) equipped multi-storey frame structure and schematic representation of a rack-and-pinion flywheel-based inerter device with *n* gearing stages.

Recognizing the importance of a comprehensive TMDI design utilizing cost-related criteria in assessing the TMDI potential for seismic protection of building structures, this paper extends the aforementioned efforts to examine the risk-informed TMDI optimization, adopting multiple objectives and using response

3

history analysis and probabilistic life-cycle criteria to quantify performance. Emphasis is placed on applications for protection of multi-storey buildings in the region of Chile. This emphasis is motivated by the fact that mass/inertia dampers have been shown to be particularly efficient in reducing structural damage potential of earthquakes generated in the Chilean seismo-tectonic environment [12], which is dominated by large magnitude seismic events yielding ground motions of long effective duration [34]. As in [12], risk quantification is accomplished through response history analysis, with seismic hazard described through use of a non-stationary stochastic ground motion model. Multiple criteria are utilized in the design optimization. The main one, representing overall direct benefits, is the life-cycle cost of the system, composed of the upfront TMDI cost (approximated here as a function of the total secondary mass) and the anticipated seismic losses over the lifetime of the structure. For enhanced decision support [35], two additional criteria are examined, both represented through response characteristic with specific probability of exceedance over the lifetime of the structure, therefore corresponding to design events with specific annual rate of exceedance. The first one corresponds to the repair cost, and incorporates risk-averse attitudes into the design process [36, 37], whereas the other corresponds to the inerter force, which incorporates practical constraints for the inerter size and the force transfer between TMDI and the supporting structure. This ultimately leads to a multi-objective formulation of the design problem with three different objectives. A variant of the design problem is also examined incorporating the inerter force (third objective) within the upfront cost in the problem formulation (adjusting first objective), leading to a dual-objective design problem. This corresponds to TMDI cost taken as function of both the secondary mass and the inerter force demand. Since costing information for the latter is not available, a parametric investigation is undertaken. For all design problems, stochastic simulation is used to estimate the necessary risk measures, whereas a Kriging metamodel is developed to support an efficient optimization process. The main novel contributions of the present work is a) TMDI optimal design and performance evaluation using life-cycle cost criteria for a real-life case study building exposed to site-specific seismic hazard represented by a non-stationary stochastic ground motion model, and b) the incorporation of the inerter force within the adopted performance evaluation framework which has been employed in the past solely for TMD applications [12]. Emphasis is placed on discussing numerical results presented in the form of Pareto fronts while most aspects of the considered probabilistic design and performance evaluation framework are only briefly reviewed with the exception of those details related to novel elements introduced to accommodate intricacies of the TMDI design problem such as the inerter force. Readers interested in further details for the adopted performance evaluation framework are directed to references [12, 35].

The remaining of the paper is organized as follows. In the next Section the equations of motion of the TMDI are presented, followed (Section 3) by a review of the adopted probabilistic framework for the performance evaluation. In Section 4 the multi-objective design is discussed, including numerical details for its implementation. Section 5 discusses a case study for an existing 21-story building in Santiago, Chile to

Ruiz R, Taflanidis AA, **Giaralis A,** Lopez-Garcia D. (2018). Risk-informed optimization of the tuned mass-damper-inerter (TMDI) for the seismic protection of multi-storey building structures**.** *Engineering Structures,* **177**: 836-850.

investigate the benefits of the TMDI (over the TMD) within the adopted design framework, as well as examine impact of the topological TMDI configuration on the performance, while Section 6 summarizes conclusions.

## 2. Equations of motion for TMDI equipped multi-storey buildings

Consider the *n*-storey planar frame building, shown in Figure 1, whose oscillatory motion due to a ground acceleration $\ddot{x}_g$ is to be suppressed (primary structure). The TMDI consists of a classical TMD located at the $i_d$-th floor of the primary structure comprising the secondary mass $m_d$ attached to the structure via a linear spring of stiffness $k_d$ and a linear dashpot of damping coefficient $c_d$. The TMD mass is linked to the $i_b$-th floor by an inerter with inertance $b$. Let $\mathbf{x}_s \in \Re^n$ be the vector of floor displacements of the primary structure relative to the ground and $\ddot{x}_g \in \Re$ be the ground acceleration. Denote by $\mathbf{R}_d \in \Re^n$ the *TMD location* vector specifying the floor the TMD is attached to (i.e., vector of zeros with a single one in its $i_d$ entry), and by $\mathbf{R}_b \in \Re^n$ be the *inerter location* vector specifying the floor the inerter is connected to (i.e., vector of zeros with a single one in its $i_b$ entry). Let, also, $y \in \Re$ be the displacement of the TMD mass relative to the $i_d$ floor and define the *connectivity* vector by $\mathbf{R}_c = \mathbf{R}_d - \mathbf{R}_b$. Then, the resisting inerter force, denoted by $F_b$ in Figure 1, is equal to

$$F_b(t) = b\left[\ddot{y}(t) + \mathbf{R}_c \ddot{\mathbf{x}}_s(t)\right] \tag{1}$$

and the coupled equations of motion for the TMDI equipped primary structure in Figure 1 modeled as lumped-mass damped multi degree-of-freedom (MDOF) system are written as

$$\left(\mathbf{M}_s + \mathbf{R}_d m_d \mathbf{R}_d^T + \mathbf{R}_c b \mathbf{R}_c^T\right)\ddot{\mathbf{x}}_s(t) + \left(m_d \mathbf{R}_d + b\mathbf{R}_c\right)\ddot{y}(t) + \mathbf{C}_s \dot{\mathbf{x}}_s(t) + \mathbf{F}_s(\mathbf{x}_s(t))$$
$$= -\left(\mathbf{M}_s + \mathbf{R}_d m_d \mathbf{R}_d^T\right)\mathbf{R}_s \ddot{x}_g(t) \tag{2}$$

$$(m_d + b)\ddot{y}(t) + \left(m_d \mathbf{R}_d^T + b\mathbf{R}_c^T\right)\ddot{\mathbf{x}}_s(t) + c_d \dot{y}(t) + k_d y(t) = -m_d \mathbf{R}_d^T \mathbf{R}_s \ddot{x}_g(t) , \tag{3}$$

where $\mathbf{M}_s \in \Re^{n \times n}$ and $\mathbf{C}_s \in \Re^{n \times n}$ are the mass and damping matrices of the primary structure, respectively, $\mathbf{F}_s(\mathbf{x}_s(t)) \in \Re^n$ is the vector or restoring forces acting on each storey and $\mathbf{R}_s \in \Re^n$ is the earthquake influence coefficient vector (vector of ones for planar structural model). For the restoring forces in the case study linear structural behavior is assumed $\mathbf{F}_s(\mathbf{x}_s(t)) = \mathbf{K}_s \mathbf{x}_s(t)$ where $\mathbf{K}_s \in \Re^{n \times n}$ is the stiffness matrix of the primary structure. This assumption of linear structural behavior is deemed to be a good approximation to the actual structural response because even under strong earthquake shaking the majority of Chilean RC buildings having 9 or more stories and built after 1985 have been observed to perform at (or close to) the "operational limit state" level [38] instead of the "life safety limit state" level assumed by the Chilean seismic design code for such excitations.

Ruiz R, Taflanidis AA, **Giaralis A,** Lopez-Garcia D. (2018). Risk-informed optimization of the tuned mass-damper-inerter (TMDI) for the seismic protection of multi-storey building structures. *Engineering Structures,* **177**: 836-850.

Eq. (3) suggests that the total inertia of the TMDI is equal to $(m_d+b)$. Hence, the TMDI frequency ratio $f_d$, damping ratio $\zeta_d$, inertance ratio $\beta$, and mass ratio $\mu$, the design variables for the configuration, are defined with respect to that total inertia as

$$f_d = \sqrt{\frac{k_d}{(m_d + b)}} / \omega_1; \quad \zeta_d = \frac{c_d}{2(m_d + b)\omega_d}; \quad \beta = \frac{b}{M}; \quad \mu = \frac{m_d}{M}, \tag{4}$$

where $\omega_1$ and $M$ are the fundamental natural frequency and the total mass of the primary structure, respectively and $\omega_d = f_d\omega_1$ represents the TMDI natural frequency.

Note that in deriving Eq. (2) the inerter is taken as massless/weightless regardless of the value of the inertance property $b$, and, therefore, it does not attract any seismic lateral force [17]. This consideration is justified by referring to a typical flywheel-based inerter device implementation shown in the inlet of Figure 1 for which the inertance $b$ is proportional to the *product of the square* of the gearing ratios, $r_k/pr_k$, $k=1,2,\dots n$, where $n$ is the number of gears used to drive a flywheel with mass $m_f$ and radius $\gamma_f$ [18, 39]. The scalability of the inertance endowed by the gearing system driving the flywheel can be readily appreciated theoretically by referring to the expression for the inertance included in Figure 1 (see also [28]). In practice, the scalability of inerter devices and the associated small physical mass over inertance ratio can be illustrated by noting that the only currently commercially available inerter for small-scale automotive applications relies on a ball-screw mechanism and achieves approximately 75kg of inertance from a device weighting 2kg [40], while the ball-screw inerter element embedded into the full-scale tuned viscous-mass-damper prototype device for seismic applications discussed by Watanabe et al. [19] achieves an apparent 5400t inertance from a device weighting only 0.75t.

## 3. Risk characterization and design metrics quantification

### 3.1 Adopted probabilistic seismic risk quantification framework and design variables

The characterization/quantification of seismic risk follows the framework initially discussed in [13]. Approach, shown in Figure 2, is implemented though use of appropriate models (modules) for the seismic excitation (hazard analysis), structural system (structural analysis) and loss evaluation (damage and loss analysis), and through adoption of appropriate probability distributions to the parameters that are considered as uncertain in these different models. The augmented $n_\theta$-dimensional vector of all such parameters is denoted by $\boldsymbol{\theta}$, the space of possible parameter values as $\Theta$ and the associated probability distribution, with support in $\Theta$, as $p(\boldsymbol{\theta})$. This distribution facilitates ultimately the seismic risk quantification, i.e. the description of the uncertainties impacting the output of each of the modules in Figure 1. Further details related to these modules within the context of the adopted framework are provided in Appendix A.

Ruiz R, Taflanidis AA, **Giaralis A,** Lopez-Garcia D. (2018). Risk-informed optimization of the tuned mass-damper-inerter (TMDI) for the seismic protection of multi-storey building structures**.** *Engineering Structures,* **177**: 836-850.
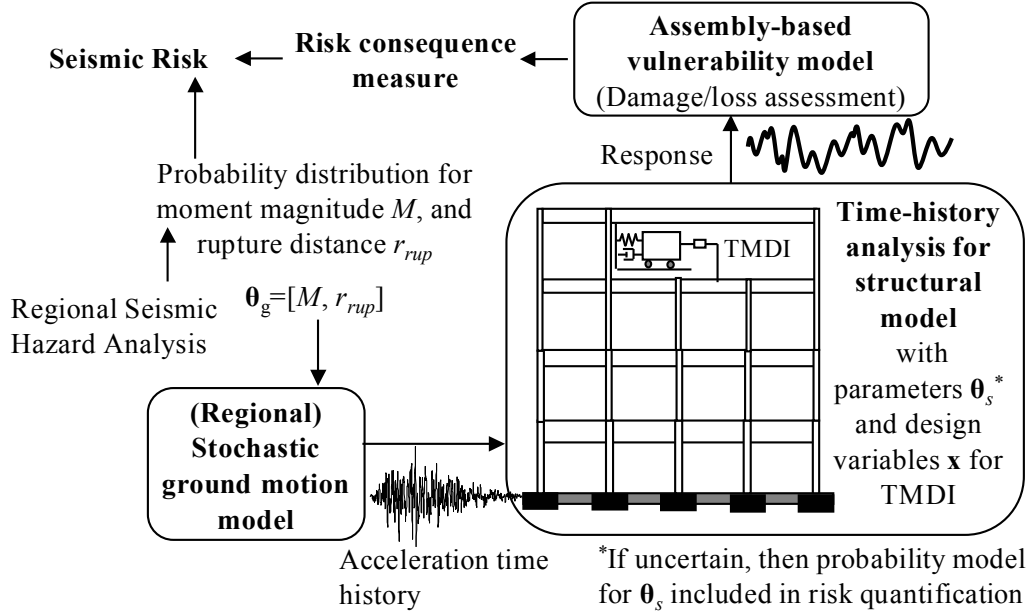
Figure 2. Overview of risk quantification and assessment approach

To formalize the design problem let the vector of controllable parameters for the TMDI referred to herein as *design variables*, be $\mathbf{x} \in X \subset \Re^{n_x}$, where $X$ denotes the admissible design space. Ultimately $\mathbf{x}$ includes the mass $m_d$ (or mass ratio $\mu$), the inertance $b$ (or inertance ratio $\beta$), the stiffness $k_d$ (or frequency ratio $f_d$), and the damping coefficient $c_d$ (or damping ratio $\zeta_d$). For a specific design configuration $\mathbf{x}$, the risk consequence measure, describing the favorability of the response from a decision-theoretic viewpoint, is given by $h_r(\mathbf{\theta}, \mathbf{x})$. This measure is dependent upon both design variables $\mathbf{x}$ and the model parameter configuration $\mathbf{\theta}$. Addressing, now, the uncertainty in the description of $\mathbf{\theta}$ leads to the desired seismic risk characterization defined as the expected value of the risk-consequence measure, $H_r(\mathbf{x})$, and mathematically described by the multi-dimensional probabilistic integral

$$H_r(\mathbf{x}) = \int_{\Theta} h_r(\mathbf{\theta}, \mathbf{x}) p(\mathbf{\theta}) d\mathbf{\theta} . \tag{5}$$

Through appropriate selection of the risk consequence measure different risk quantifications can be addressed within the adopted framework, supporting the estimation of all desired design metrics. The herein proposed metrics which serve for optimal TMDI design objectives are discussed next and their corresponding risk consequence measures to be used in conjunction with Eq.(5) are defined.

### 3.2 Risk metrics for optimal TMDI design and definition of their consequence measures

#### 3.2.1 Life cycle cost metric

The main metric utilized in the proposed TMDI design formulation is the total expected life-cycle cost $C(\mathbf{x})=C_i(\mathbf{x})+C_l(\mathbf{x})$, provided by adding the initial (upfront) cost $C_i(\mathbf{x})$, which is a function of the TMDI characteristics, and the expected cost due to earthquake losses over the life-cycle of the structure $C_l(\mathbf{x})$. Under

Ruiz R, Taflanidis AA, **Giaralis A,** Lopez-Garcia D. (2018). Risk-informed optimization of the tuned mass-damper-inerter (TMDI) for the seismic protection of multi-storey building structures**.** *Engineering Structures,* **177**: 836-850.

the Poisson assumption of earthquake occurrence, as considered in the case study, the present value $C_l(\mathbf{x})$ of expected future seismic losses is given by integral of Eq. (5) with associated risk consequence measure definition [41]

$$h_r(\boldsymbol{\theta}, \mathbf{x}) = C_r(\boldsymbol{\theta}, \mathbf{x}) v t_{life} \left[ (1 - e^{-r_d t_{life}}) / (r_d t_{life}) \right], \tag{6}$$

where $r_d$ is the discount rate, $t_{life}$ is the life cycle considered, $v$ is the annual frequency of occurrence of earthquake events and $C_r(\boldsymbol{\theta}, \mathbf{x})$ is the cost given the occurrence of an earthquake event, estimated through an assembly-based vulnerability approach as detailed in Appendix A [42].

### *3.2.2 Risk aversion metric*

Consideration of only the expected life-cycle cost as performance objective facilitates what is commonly referenced as "*risk-neutral*" design. The latter assumes that preference is assessed only through the average losses/consequences. Nevertheless, in many cases, accounting for alternative risk perceptions leading to more conservative designs (*risk aversion*) is deemed desirable, since *risk-neutral* design does not explicitly address the unlikely but potentially devastating losses that lie towards the tail of the losses/consequence distribution [36]. To this end, the incorporation of an additional performance objective corresponding to repair cost, $C_{thresh}$, with specific probability of exceedance over the life-cycle of the structure was proposed in [35] as a means to address risk aversion attitude to the TMDI design problem formulation. This is adopted here as an additional design risk metric. Based on the Poisson assumption of seismic events, the probability of the repair cost $C_r$ exceeding the targeted threshold $C_{thresh}(\mathbf{x})$ metric over the considered lifetime of the structure is

$$P[C_r > C_{thresh}(\mathbf{x}) \,|\, \mathbf{x}, t_{life}] = 1 - \exp^{-t_{life} v \cdot P[C_r > C_{thresh}(\mathbf{x}) | \mathbf{x}, \text{ seismic event}]}, \tag{7}$$

where $P[C_r > C_{thresh}(\mathbf{x}) \,|\, \mathbf{x}, \text{ seismic event}]$ is the probability of exceeding the repair threshold given that a seismic event has occurred. The probability $P[C_r > C_{thresh}(\mathbf{x}) \,|\, \mathbf{x}, \text{ seismic event}]$ is given by the generic risk integral of Eq. (5) with risk consequence measure

$$h_r(\boldsymbol{\theta}, \mathbf{x}) = I_C(\boldsymbol{\theta}, \mathbf{x}), \tag{8}$$

corresponding to an indicator function, being one if $C_r(\boldsymbol{\theta}, \mathbf{x}) > C_{thresh}(\mathbf{x})$ and zero otherwise. Details about numerical estimation of the integral are provided in Section 4.2 and Appendix A.

### *3.2.3 Inerter-specific metric*

As discussed in the introduction, efficient vibration suppression using optimal TMDI configurations [21, 26] relies on large inertance values and entails large inerter forces which need to be transferred to the host structure. Accommodation of these forces necessitates pertinent local strengthening of structural elements supporting the inerter. This consideration requires detailed knowledge of the cost associated with large-scale inerter implementation and installation which should naturally add to the overall TMDI upfront cost, $C_i(\mathbf{x})$. Nevertheless, such knowledge is currently unavailable since inerter devices tailored for civil engineering

Ruiz R, Taflanidis AA, **Giaralis A,** Lopez-Garcia D. (2018). Risk-informed optimization of the tuned mass-damper-inerter (TMDI) for the seismic protection of multi-storey building structures. *Engineering Structures,* **177**: 836-850.

applications are not commercially available. To circumvent the above lack of knowledge, an approximation is established in which a separate non-monetary design metric is considered within the adopted seismic risk framework, namely the reference *inerter force* $F_{thresh}$ developing during a specific design seismic event, while no inerter-related cost is added to the TMDI upfront cost $C_i(\mathbf{x})$. Note that this is similar to the approach adopted for quantifying the reference capacity for other type of protective devices, such as fluid viscous dampers [43]. The design seismic event is specified by considering the inerter force with specific probability of exceedance over the life-cycle of the structure $P[F_b > F_{thresh}(\mathbf{x})\,|\,\mathbf{x}, t_{life}]$. Under the stated assumptions, this probability is given by an equation similar to Eq. (7),

$$P[F_i > F_{thresh}(\mathbf{x})\,|\,\mathbf{x}, t_{life}] = 1 - \exp^{-t_{life} v \cdot P[F_i > F_{thresh}(\mathbf{x})|\mathbf{x},\text{ seismic event}]} \tag{9}$$

where $P[F_i > F_{thresh}(\mathbf{x})\,|\,\mathbf{x}, \text{seismic event}]$ is given by the generic risk integral of Eq. (5) with risk consequence measure

$$h_r(\boldsymbol{\theta}, \mathbf{x}) = I_i(\boldsymbol{\theta}, \mathbf{x}), \tag{10}$$

corresponding to $h_r(\boldsymbol{\theta}, \mathbf{x}) = I_i(\boldsymbol{\theta}, \mathbf{x})$, being one if $F_i(\boldsymbol{\theta},\mathbf{x}) > F_{thresh}(\mathbf{x})$ and zero otherwise.

## 4. Multi-objective risk informed design

### 4.1 Problem formulation

The three risk metrics detailed in the previous section are herein used as the objectives in formulating the TMDI design problem. In this respect, the multi-criteria design problem is expressed ultimately as

$$\mathbf{x}^* = \arg\min_{\mathbf{x} \in X} \left\{ C(\mathbf{x}) = C_i(\mathbf{x}) + C_l(\mathbf{x}), C_{thresh}(\mathbf{x}), F_{thresh}(\mathbf{x}) \right\}^T$$
$$\text{such that } P[C_r > C_{thresh}(\mathbf{x})\,|\,\mathbf{x}, t_{life}] = p_{or} \tag{11}$$
$$P[F_i > F_{thresh}(\mathbf{x})\,|\,\mathbf{x}, t_{life}] = p_{oi},$$

where $C(\mathbf{x})$ [first objective] is the life-cycle cost, $C_{thresh}(\mathbf{x})$ [second objective] is the repair threshold with probability of being exceeded $p_{or}$ over the lifetime of the structure and $F_{thresh}(\mathbf{x})$ [third objective] is the inerter force with probability of being exceeded $p_{oi}$ over the lifetime of the structure. This multi-objective formulation leads ultimately to a set of points (also known as dominant designs) that lie on the boundary of the feasible objective space and form a manifold: the Pareto front. A point belongs to the Pareto front and it is called Pareto optimal point if there is no other point that improves one objective without detriment to any other. Example of Pareto fronts will be provided in the case study later. The multi-objective problem allows for the identification of a range of TMDI configurations (Pareto optimal solutions) striking a trade-off among (i) total cost $C(\mathbf{x})$, (ii) consequences of events $C_{thresh}(\mathbf{x})$ and (iii) inerter force $F_{thesh}(\mathbf{x})$. The first objective is estimated within a life-cycle setting whereas the other two as values corresponding to a design event having specific annual rate of exceedance, defined through $p_{or}$ and $p_{oi}$. The selection of probabilities $p_{or}$ and $p_{oi}$ allows the designer to incorporate different risk attitudes within the problem formulation. For example, risk-averse

Ruiz R, Taflanidis AA, **Giaralis A,** Lopez-Garcia D. (2018). Risk-informed optimization of the tuned mass-damper-inerter (TMDI) for the seismic protection of multi-storey building structures. *Engineering Structures,* **177**: 836-850.

attitude of different level (i.e., as desired by the decision maker) can be achieved by focusing on events towards the tails of the respective distributions for $C_r$ and/or $F_i$. Once the Pareto front described by Eq. (11) has been identified, the designer or decision maker (e.g. building owner) can ultimately make the final decision among the Pareto optimal solutions, accounting for any further practical considerations such as architectural constraints for the TMDI implementation (accommodation of larger secondary mass with increased volume).

A variant of this design problem is also examined in the case study by incorporating $F_{thresh}(\mathbf{x})$ in the upfront TMDI cost, rather as separate objective (see also discussion in section 3.2.3). This reduces the design problem to a bi-objective optimization. As no detailed costing information is available for the relationship between $C_i(\mathbf{x})$ and $F_{thresh}(\mathbf{x})$ a parametric investigation will be performed. This variant formulation of the design problem is examined primarily to investigate generic trends, as comprehensive performance assessment based on it requires a more detailed characterization of the upfront cost associated with the inerter force demand.

### 4.2 Computational approach for design optimization

Optimization of Eq. (11) requires different risk metrics, $C(\mathbf{x})$, $C_{thresh}(\mathbf{x})$, and $F_{thresh}(\mathbf{x})$, whose estimation involves calculation of probabilistic integrals of the form of Eq. (5). Stochastic simulation is adopted here for this estimation: using a finite number, $N$, of samples of $\mathbf{\theta}$ drawn from proposal density $q(\mathbf{\theta})$, an estimate for the risk integral of interest (expressed through generalized form of Eq. (5)) is

$$\hat{H}_r(\mathbf{x}) = \frac{1}{N} \sum_{j=1}^{N} h_r(\mathbf{x}, \mathbf{\theta}^j) \frac{p(\mathbf{\theta}^j)}{q(\mathbf{\theta}^j)} \quad , \tag{12}$$

where $\mathbf{\theta}^j$ denotes the sample used in the $j^{th}$ simulation and $\{\mathbf{\theta}^j; j=1,\ldots,N\}$ represents the entire sample-set. The proposal density $q(\mathbf{\theta})$ is used to improve the efficiency of this estimation (i.e., reduce the coefficient of variation in the estimate), by focusing the computational effort on regions of the $\Theta$ space that contribute more to the integrand of the probabilistic integral in Eq. (5) following the concept of Importance Sampling (IS). Further details on IS implementation for seismic applications can be found in [13]. The efficient estimation of $C_{thresh}(\mathbf{x})$ and $F_{thresh}(\mathbf{x})$ using Eq. (12) involves the solution of an inverse problem (i.e., the identification of the threshold corresponding to a specific probability) and is discussed in Appendix A.

The design problem in Eq. (11) is solved by substituting the stochastic simulation estimates, obtained through use of Eq. (12), for the required probabilistic integrals. The existence of the stochastic simulation error within the optimization is addressed by adopting an exterior sampling approach [44], utilizing the same, sufficiently large, number of samples throughout all iterations in the optimization process. That is, $\{\mathbf{\theta}^j; j=1,\ldots,N\}$ in Eq. (12) is chosen the same for each design configuration examined. In this manner, the relative importance of the estimation error is reduced in the comparison of different design choices by creating a consistent error throughout all design points. Coupled with the IS approach for reducing the absolute

importance of the estimation error (i.e. obtain higher accuracy estimates), the above sampling strategy removes any influence of the stochastic simulation error on the identified Pareto optimal solutions.

Furthermore, in supporting an efficient optimization, an approach relying on Kriging surrogate modeling is adopted following the guidelines discussed in [43]. The surrogate model is established here to provide an approximate relationship between the design selection **x** (input to the surrogate model) and the risk quantities needed in the optimization of Eq. (11), $C_{thresh}(\mathbf{x})$, $F_{thresh}(\mathbf{x})$, and $C_l(\mathbf{x})$ (outputs for the surrogate model). The model is developed using the following approach. A large set of design configurations for the TMDI is first established to serve as training points for developing the Kriging metamodel, utilizing latin hypercube sampling in domain $X^m$. The latter domain $X^m$ is chosen to be equal to or larger than the admissible design space $X$. For each such design configuration (training point) the risk quantities $C_{thresh}(\mathbf{x})$, $F_{thresh}(\mathbf{x})$, and $C_l(\mathbf{x})$ are calculated through stochastic simulation as detailed earlier. Using this information the Kriging metamodel is developed to provide highly efficient (thousands of evaluations within seconds) approximations to the risk measures of interest, $\tilde{C}$ , $\tilde{l}$ and $\tilde{C}$ , for any **x** within $X^m$ (the domain considered for the metamodel development). These approximations are used to replace $C_{thresh}(\mathbf{x})$, $F_{thresh}(\mathbf{x})$, and $C_l(\mathbf{x})$ within the multi-objective optimization of Eq. (11). Note that formulation of that optimization requires, additionally, an appropriate assumption for the upfront damper cost (used to calculate the overall cost $C$). The multi-objective problem is ultimately solved through any desired numerical method, for example through a blind-search approach or through genetic algorithms [45]. Leveraging the high computational efficiency of the surrogate model approximation, the optimization is efficiently performed, even through numerical schemes that require very large number of evaluations of the different objectives. Further details for the metamodel formulation are available in [43].

## 5. Application to a real-life case study structure

As case study, the design of a TMDI for a 21-story existing reinforced concrete (RC) building located in Santiago, Chile is considered [46]. The building has tapered elliptical shape, length 76.2 m and average depth 20 m (varying across its length). A pendulum-like TMD is installed on the last floor acting along the slender axis of the building. In this regard, single-axis TMD(I) design variations are examined here considering adopting a planar model along the building slender axis as the primary structure. A schematic of the building is shown in Figure 3.

### 5.1 Model and cost characteristics

A linear structural model detailed in [12] is taken as the primary structure. As mentioned earlier the assumption of linear structural response is deemed to be a reasonable approximation to the actual behavior given that only 2% out of 1939 RC buildings having 9 or more stories and built between 1985 and 2009 suffered significant damage during the 2010 seismic event off the coast of central Chile with Magnitude 8.8 [38]. The total mass of the structure is 33.169.000 kg and Rayleigh damping is utilized by assigning an equal

Ruiz R, Taflanidis AA, **Giaralis A,** Lopez-Garcia D. (2018). Risk-informed optimization of the tuned mass-damper-inerter (TMDI) for the seismic protection of multi-storey building structures. *Engineering Structures,* **177**: 836-850.

damping ratio for the first and second mode with 3% nominal value. The natural periods and modal participating mass ratios in parenthesis for the first three modes are 2.10s (77%), 0.54s (16%) and 0.25s (5%). For the loss assessment model three different damageable assemblies are examined: partitions, ceiling, and contents. For the first one, the *EDP* (engineering demand parameter) is taken as the peak inter-story drift and for the latter two as the peak floor acceleration. Note that damages to structural components are not included in this study since, as discussed above, they are expected to have small contribution. Lognormal fragilities are considered for all damages states. The fragility and repair cost characteristics are the same as in [12] and are reviewed in Table 1.

Table 1. Characteristics of fragility curves and expected repair cost and time for each story.

| Damage state | EDP | $\beta_f$[+++] | $\sigma_f$[+++] | $n_{el}$[++] | Repair cost ($\$/n_{el}$) |
|---|---|---|---|---|---|
| *Partitions* | | | | | |
| 1(small cracks) | IDR[+] | 0.21% | 0.60 | 350 m$^2$ | 22.30 |
| 2(moderate cracks) | IDR | 0.71% | 0.45 | 350 m$^2$ | 60.30 |
| 3(severe damage) | IDR | 1.2% | 0.45 | 350 m$^2$ | 92.70 |
| *Contents* | | | | | |
| 1(damage) | PFA[+] | 0.70g | 0.30 | 100 | 1000 |
| *Ceiling* | | | | | |
| 1(some tiles fallen) | PFA | 0.55g | 0.40 | 1500 m$^2$ | 15.20 |
| 2(extensive tile fallout) | PFA | 1.00g | 0.40 | 1500 m$^2$ | 120.10 |
| 3(total ceiling collapse) | PFA | 1.50g | 0.40 | 1500 m$^2$ | 237.70 |

[+]IDR: Peak interstory drift; PFA: Peak floor acceleration
[++]$n_{el}$: number of elements per story
+++ $\beta_f$, $\sigma_f$: median and logarithmic standard deviation, respectively, for definition of fragility curve

For the seismic hazard characterization seismic events occurrences are assumed to follow a Poisson distribution and so are history independent. The uncertainty in moment magnitude $M$ is modeled by the Gutenberg-Richter relationship truncated on the interval $[M_{min}, M_{max}] = [5.5, 9.0]$, (events smaller than $M_{min}$ do not contribute to the seismic risk) which leads to $p(M) = b_M e^{-b_M M}/(e^{-b_M M_{min}} - e^{-b_M M_{max}})$ and expected number of events per year $v = e^{a_M - b_M M_{min}} - e^{a_M - b_M M_{max}}$. The regional seismicity factors $b_M$ and $a_M$ are chosen by averaging the values for the seismic zones close to Santiago based on the recommendations in [47]. This results to $b_M$=0.8log$_e$(10) and $a_M$=5.65log$_e$(10). Regarding the uncertainty in the event location, the closest distance to the fault rupture, $r_{rup}$, for the earthquake events is assumed to follow a beta distribution in [30 250] km with median $r_{med}$=100 km and coefficient of variation 35%. For modeling the excitation the compatible with the regional hazard [34] site-based, stochastic ground motion model developed in [12] is adopted. The probability models for $M$ and $r_{rup}$ along with adopted stochastic ground motion model result in peak ground acceleration (PGA) with probability of exceedance 10% in 50 years equal to 0.45 g, which is in agreement with literature results for Santiago [48].

Ruiz R, Taflanidis AA, **Giaralis A,** Lopez-Garcia D. (2018). Risk-informed optimization of the tuned mass-damper-inerter (TMDI) for the seismic protection of multi-storey building structures**.** *Engineering Structures,* **177**: 836-850.

Uncertainty is included only in the seismic hazard characterization, with parameters for the structural model taken as deterministic. This should be deemed a reasonable assumption since a linear structural model is utilized in the analysis, for which response variability due to uncertainty in structural parameters is small when compared to variability stemming from seismic hazard [22, 49, 50]. This means that vector $\boldsymbol{\theta}$ consists of $M$, $r_{rup}$ and the white noise sequence involved in the stochastic ground motion model.

The discount rate is taken equal to 1.5% and the lifetime $t_{life}$ is assumed to be 50 years. The repair cost and inerter force thresholds are taken to correspond to probability $p_{oi}=p_{or}=10\%$ over $t_{life}$. This choice is equal to return rate of 475 years, which is a standard definition for the most-credible design event in modern seismic codes. This selection shifts focus for objective 2 and 3 thresholds away from the median and towards the tail of the respective distributions for $C_r$ and $F_i$. The life-cycle cost and $C_{thresh}$ for the uncontrolled structure are, respectively, \$2.02x10$^6$ and \$1.13x10$^6$. For the main design problem formulation the upfront TMDI cost is based on the attached mass. The underlying assumption is that the inerter and damper cost is by comparison negligible. This cost is approximated to be linearly related to the TMDI mass $C_i(\mathbf{x})=b_c m$ [12] with value of $b_c$ equal to 2500 \$/ton. This value is taken based on [51], additionally considering here that implementation is unidirectional and has no smart components (purely passive application). Modifications of the upfront cost for the variant design problem will be discussed later.

## 5.2 Design and optimization details

Seven different topological configurations are examined in which the secondary mass is attached to either the top floor ($i_d$=21) or the 18$^{th}$ floor ($i_d$=18) and the inerter connected to one of the three floors below for $i_d$=21, $i_b$=20, $i_b$=19, $i_b$=18, respectively, and one of the two floors above or below for $i_d$=18, $i_b$=20, $i_b$=19, $i_b$=17, $i_b$=16, respectively. The different topologies will be distinguished, herein, using their respective $i_d$, $i_b$ values. As discussed earlier, the design vector includes the inertance ratio $\beta$, the mass ratio $\mu$, the damping ratio $\zeta_d$ and the frequency ratio $f_d$. The admissible domain $X$ for the first two design variables is taken as [0.1 5] for $\beta$ and [0.1 1.0] % for $\mu$. Larger values for the inertance lead to unreasonable large inerter forces whereas for the mass ratio, values greater than 1.0% are impractical (significant addition of gravity loads concentrated on a specific floor) and values lower than 0.1% are too small for practical implementation. The upper limit for $\beta$ range is justified by the potential of having a sufficient number of inerters arranged in parallel with each one having several thousands of tons of inertance through appropriate gearing, as discussed in Section 2. The large range for $\beta$ was chosen to get a complete representation of the Pareto front, as this parameter is critical, as will be shown later, in impacting the TMDI performance for all objectives. For the remaining two design variables the admissible design domain is set to [0.005 1.1] for $\zeta_d$ and [0.01 1.5] for $f_d$. These ranges were chosen large enough so that Pareto optimal solutions do not lie on the boundary. A total of $N$=10,000 samples are used for the stochastic simulations to calculate the different risk metrics with importance sampling densities same as the ones discussed in [12]. This selection leads to coefficient of variation for the stochastic simulation below 5% for all examined metrics. Coupled with the exterior sampling approach, this accuracy

Ruiz R, Taflanidis AA, **Giaralis A,** Lopez-Garcia D. (2018). Risk-informed optimization of the tuned mass-damper-inerter (TMDI) for the seismic protection of multi-storey building structures**.** *Engineering Structures,* **177**: 836-850.

should be considered high enough so that quality of identified Pareto front is not impacted by the stochastic simulation error.

Seven different metamodels, one for each different topological configuration, each with 6400 training points are built. The domain for the metamodel development $X^m$ is adopted as superset of $X$, corresponding to ranges [0.02 5.3] for $\beta$, [0.05 1.05] % for $\mu$, [0.005 1.1] for $\zeta_d$ and [0.01 1.5] for $f_d$. The extension or ranges for $\beta$ and $\mu$ (compared to $X$ definition) was deemed necessary after initial results showed that optimal configurations lay on the boundary of $X$. Since metamodel accuracy is lower at its boundary (smaller number of training points closer to the boundary compared to the interior points of domain $X^m$), if $X^m$ was chosen identical to $X$ this lower accuracy would had impacted the quality of the identified front, producing potentially erroneous solutions; optimal with respect to metamodel but not with respect to the exact numerical model. Extension of $X^m$ at these boundaries avoids such challenges. The outputs approximated by the metamodel correspond to $C_{thresh}(\mathbf{x})$, $F_{thresh}(\mathbf{x})$ and $C_l(\mathbf{x})$.

The accuracy of the metamodels is high, with correlation coefficient, evaluated using leave-one-out cross validation [52], close to 98-99% for all approximated response quantities. This very high accuracy should be considered sufficient for performing optimization of Eq. (11) using the metamodel approximation. Two different implementations of the optimization are considered. In the first implementation a specific value of the inertance is assumed and optimization is performed over the remaining design variables. This specific choice was made to better examine the impact of $\beta$ on the optimal TMDI configurations. The respective values used for $\beta$ are 0.1, 0.5, 1 and 3. In the second implementation all design variables are simultaneously optimized. This implementation will be referenced as $\beta$=cont herein. The Pareto fronts (optimal design points as of Eq. (11)) are identified using a blind-search: 2 million candidate design configurations for $\mathbf{x}$ are defined within the admissible domain $X$ using Latin hypercube sampling, performance objectives are estimated (using the developed metamodel) for all of them, and the Pareto front is identified by selecting the dominant designs among these configurations. The large value of candidate design configurations examined for $\mathbf{x}$ ultimately gives features of exhaustive-search to the adopted numerical scheme, facilitating convergence to the actual Pareto front. Note that half of the 2 million samples are taken in range of 0.1-0.2% for $\mu$ since it was found (also shown in the figures later) that the Pareto optimal solutions converge to that boundary.

### 5.3 Results and discussion for main design problem

Discussion first focuses on what one would consider the typical TMD configuration [17] with secondary mass attached at the top floor ($i_d$=21). Comparison with the TMD application ($\beta$=0) is also considered. For the TMD the design/performance results are taken directly from [12]. Note that $F_{thresh}(\mathbf{x})$=0 for the TMD, so the Pareto front is bi-objective. Optimal design results are presented in Figures 4-7. Figure 4 shows the Pareto front for three objectives [$C_l(\mathbf{x})$, $C_{thresh}(\mathbf{x})$, $F_{thresh}(\mathbf{x})$] and different TMD(I) configurations. Only the continuously varying $\beta$ case is presented. Figure 5 presents the projection of this front on the $C_{thresh}(\mathbf{x})$-$F_{thresh}(\mathbf{x})$, the $C_l(\mathbf{x})$-$F_{thresh}(\mathbf{x})$ and $C_l(\mathbf{x})$-$C_{thresh}(\mathbf{x})$ planes, while optimal values for $\mu$, $\zeta_d$, $f_d$ and $\beta$ along the

Ruiz R, Taflanidis AA, **Giaralis A,** Lopez-Garcia D. (2018). Risk-informed optimization of the tuned mass-damper-inerter (TMDI) for the seismic protection of multi-storey building structures. *Engineering Structures,* **177**: 836-850.

Pareto front (expressed as a function of $C_{thresh}(\mathbf{x})$) are reported in Figure 6 for $i_b$=20 and Figure 7 for $i_b$=18 (trends for $i_b$=19 fall in-between so not reported here due to space constraints) .

The results show that the addition of the TMDI can provide a significant reduction for $C_l(\mathbf{x})$ and $C_{thresh}(\mathbf{x})$, with the benefits increasing for larger inertance values. They also validate the efficiency of the TMDI compared to the classical TMD as reported in the literature before [17, 22, 26]. The front with respect to the $[C_l(\mathbf{x}), C_{thresh}(\mathbf{x})]$ objectives (third column in Figure 5) exhibits an interesting behavior as the two objectives are not competing: simultaneous reduction of both the life-cycle cost and the repair cost is feasible. This is not the case for the TMD, for which reduction of one objective cannot be accomplished without increase of the other along the Pareto front, and clearly demonstrates the mass amplification benefits endowed by the inerter to the TMD. By adjusting the remaining characteristics of the TMDI, enhanced vibration suppression is feasible without any increase of its mass. Since the upfront cost is only related to the TMDI mass, this ability enables the reduction of the repair cost without an increase of the upfront cost and therefore reduction also of the life-cycle cost. The optimal TMDI mass (Figures 6, 7) remains close to its minimum considered value across the entire front. This is not the case for the TMD for which the mass is the main design variable varying along the front, and so distinguishing the design configurations, with $\zeta_d$ and $f_d$ simply taking optimal tuning values for the respective mass ratio. Proximity of $\mu$ to its admissible boundary also demonstrates the importance of the extension of the metamodel domain $X^m$ , compared to the admissible design domain $X$, discussed in the previous section.

As expected, the increase in protection efficiency comes with a corresponding increase for the force that needs to be accommodated (larger $F_{thresh}$). This objective competes with the other two, demonstrating the value of the multi-criteria optimization for exploring all candidate solutions that provide different compromises between the TMDI performance objectives. Note, additionally, that a plateau is reached for the seismic risk with respect to the $F_{thresh}(\mathbf{x})$ objective (first two columns of Figure 4); beyond certain value for $F_{thresh}$ (different for each $\beta$ case) small benefits are obtained for $C_l(\mathbf{x})$ and $C_{thresh}(\mathbf{x})$ for significant increase of $F_{thresh}$. This feature, which is common in multi-objective design problems (i.e. large deterioration of one objective for small only benefits for the competing objectives), should be carefully evaluated when making final design decisions.

Comparing the curves corresponding to different $\beta$ values, it is observed that larger $\beta$ values lead to "wider" fronts and, therefore, to greater potential variation across the objectives, while the fronts are also overlapping in some ranges. The case with $\beta$=cont overlaps the other three ones, and has fundamentally different optimal values for the remaining TMDI design variables (Figures 6, 7). This shows that adjustment of the tuning characteristics ($\zeta_d$ and $f_d$) of the TMDI can facilitate similar performance across some ranges of the examined objectives independent of the inertance value. This demonstrates the importance of carefully examining the impact of the inertance on the established performance, considering all practical constraints with respect to the available inerter devices.  It is important to note that, contrary to the TMD implementation,

Ruiz R, Taflanidis AA, **Giaralis A,** Lopez-Garcia D. (2018). Risk-informed optimization of the tuned mass-damper-inerter (TMDI) for the seismic protection of multi-storey building structures**.** *Engineering Structures,* **177**: 836-850.

significant variation is reported for the optimal $\zeta_d$ and $f_d$ values along the Pareto front, especially when $\beta$ is also taken as design variable. This should be also attributed to the fact that based on definitions of Eq. (4), $\beta$ value impacts both $\zeta_d$ and $f_d$. Inertance ratio $\beta$ itself also demonstrates same trend of significant variability along the front. This shows the importance of carefully examining all TMDI characteristics, $\zeta_d$, $f_d$ and $\beta$ for deciding on the design configuration, and that, furthermore, this should be done with respect to the targeted objective (represented by the different Pareto optimal solutions in this case).

Discussion now moves to the comparison between the different TMDI topological configurations. For this reason results for all seven examined TMDI configurations are reported jointly in Figures 8-11, following same format as in Figures 4-6. Due to space constraints focus is placed only on the $\beta$=cont case as trends for specific $\beta$ values are same as reported above.

With respect to the topological configuration, connection of inerter to a lower floor provides significantly better behavior across all examined objectives and with fundamentally different optimal design configurations. When $i_d$=21 $C_l(\mathbf{x})$ and $C_{thresh}(\mathbf{x})$ are reduced for $i_b$=19 (compared to $i_b$=20) or $i_b$=18 (compared to $i_b$=19). When $i_d$=18 same pattern holds for $i_b$=16 (compared to $i_b$=17). This patterns agrees with the trends reported in [22] considering a simplified stationary response. Additionally, the results here show that the $F_{thresh}$ is also reduced for the smaller $i_b$ values, meaning that enhanced protection is offered with a smaller demand with respect to the forces that need to be accommodated. This stresses the importance of connecting the inerter to the lowest floor possible compare to the secondary mass, subject of course to architectural constraints. This overall behavior agrees with trends that have been reported for viscous dampers [53], and should be attributed, as proven in the viscous damper case [53], to the greater relative acceleration, due to the lower level of correlation of motions, across the end points of the inerter created when the TMDI configuration spans larger number of floors (for viscous dampers this refers to relative velocity). Connection of the inerter to a higher floor rather than a lower floor (compare for $i_d$=18 case $i_b$=17 to $i_b$=19 or case $i_b$=17 to $i_b$=20) shows a deterioration of the protection efficiency [$C_l(\mathbf{x})$ and $C_{thresh}(\mathbf{x})$ values] but not to such a significant degree as in [22], and more importantly not over the entire Pareto front. For smaller $F_{thresh}(\mathbf{x})$ values connection to a higher floor provides practically identical performance to the connection to a lower floor. This demonstrates that the structure as well as the performance objectives considered, especially the consideration of limitations on the damper force, do have an impact on the behavior when examining the connection of the inerter to a higher as opposed to a lower floor, though the overall recommendation still remains the same as in [22] for connection to a lower floor.
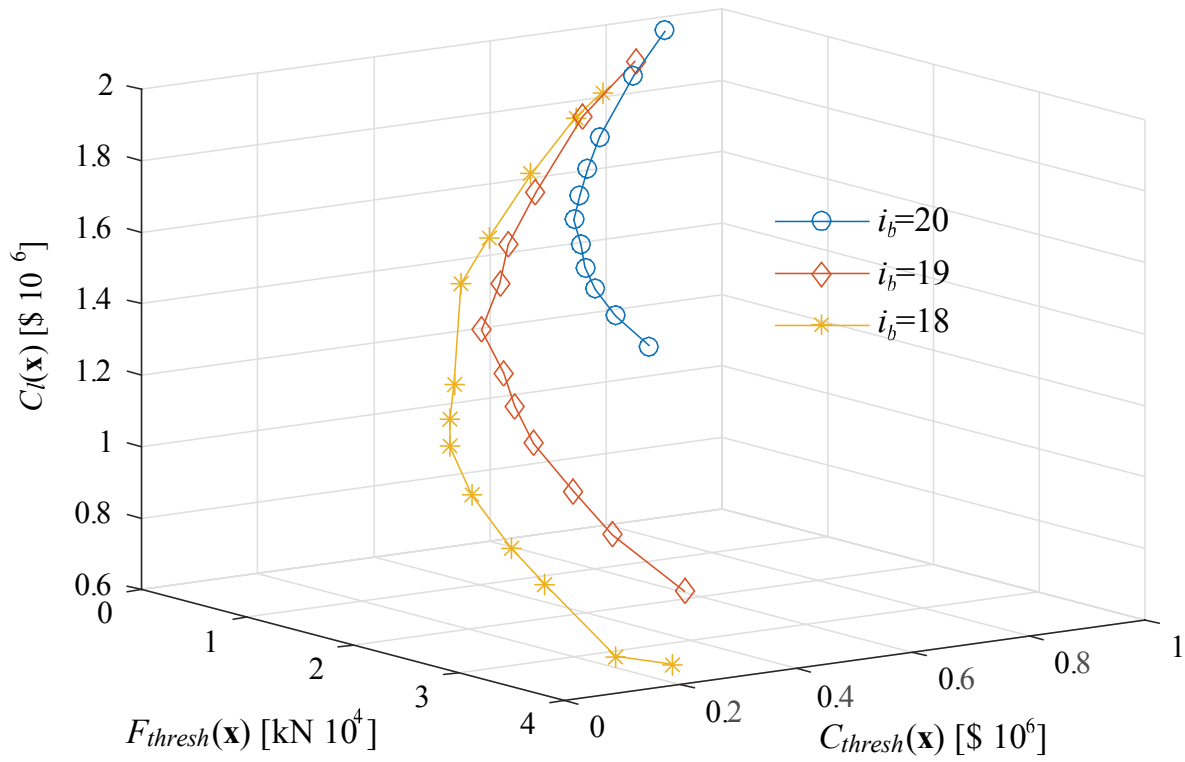
Ruiz R, Taflanidis AA, **Giaralis A,** Lopez-Garcia D. (2018). Risk-informed optimization of the tuned mass-damper-inerter (TMDI) for the seismic protection of multi-storey building structures**.** *Engineering Structures,* **177**: 836-850.

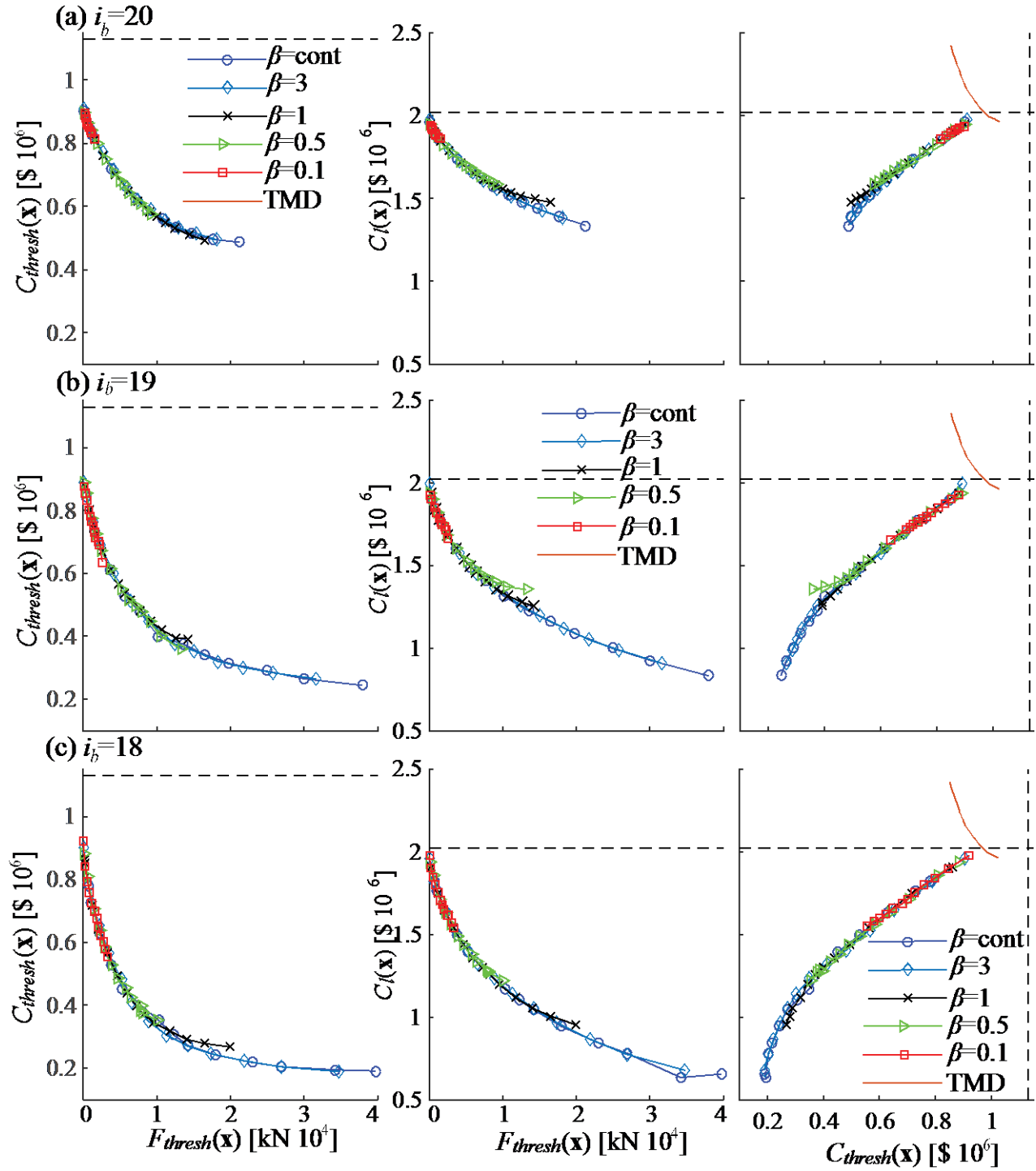Figure 4. Pareto front in the three-objective space for topological configurations with $i_d$=21.

Figure 5. Projection of the Pareto front along pair of objectives (each case presented for different $\beta$ values) for topological configurations with $i_d$=21. First row corresponds to $i_b$=20, second to $i_b$=19 and third to $i_b$=18. Dashed lines correspond to the performance of the structure without the TMDI.
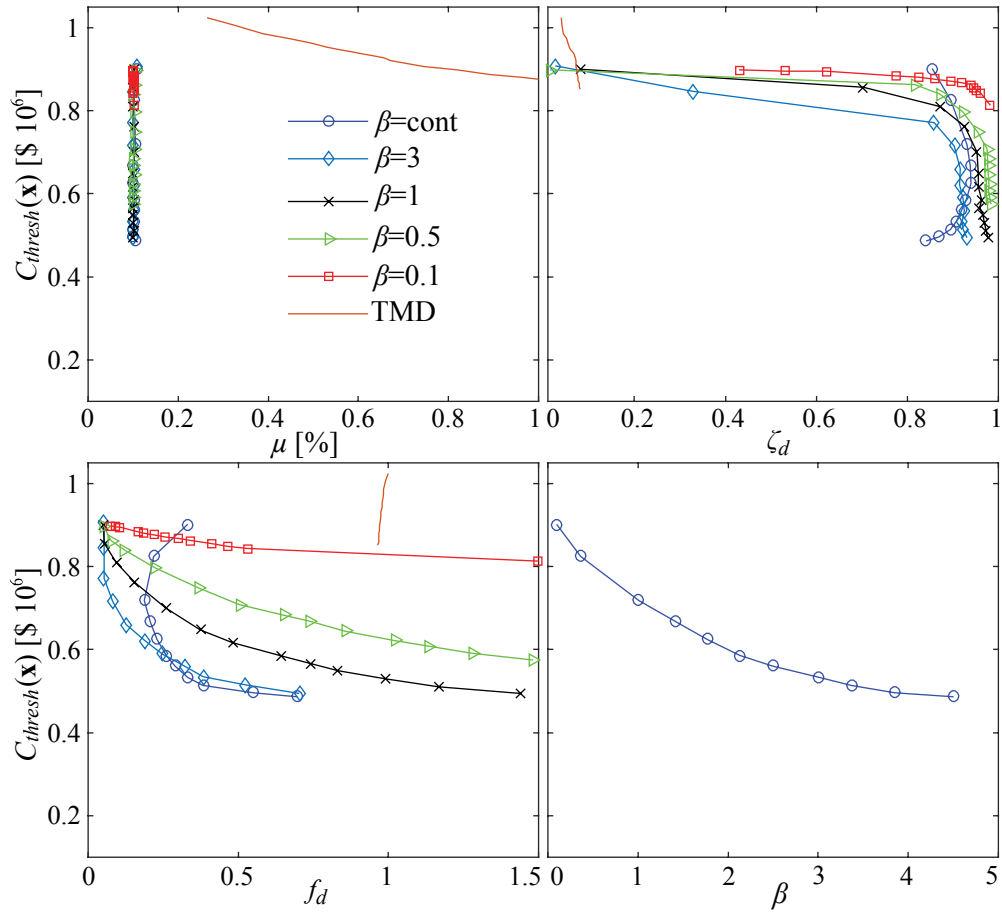
Ruiz R, Taflanidis AA, **Giaralis A,** Lopez-Garcia D. (2018). Risk-informed optimization of the tuned mass-damper-inerter (TMDI) for the seismic protection of multi-storey building structures**.** *Engineering Structures,* **177**: 836-850.

Figure 6. Optimal values for $\mu$, $\zeta_d$, $f_d$ and $\beta$ along the Pareto front [design variables are plotted with respect to the corresponding value of $C_{thresh}(\mathbf{x})$] for $i_d$=21 and $i_b$=20 TMDI configuration. Optimal TMD variables also shown.
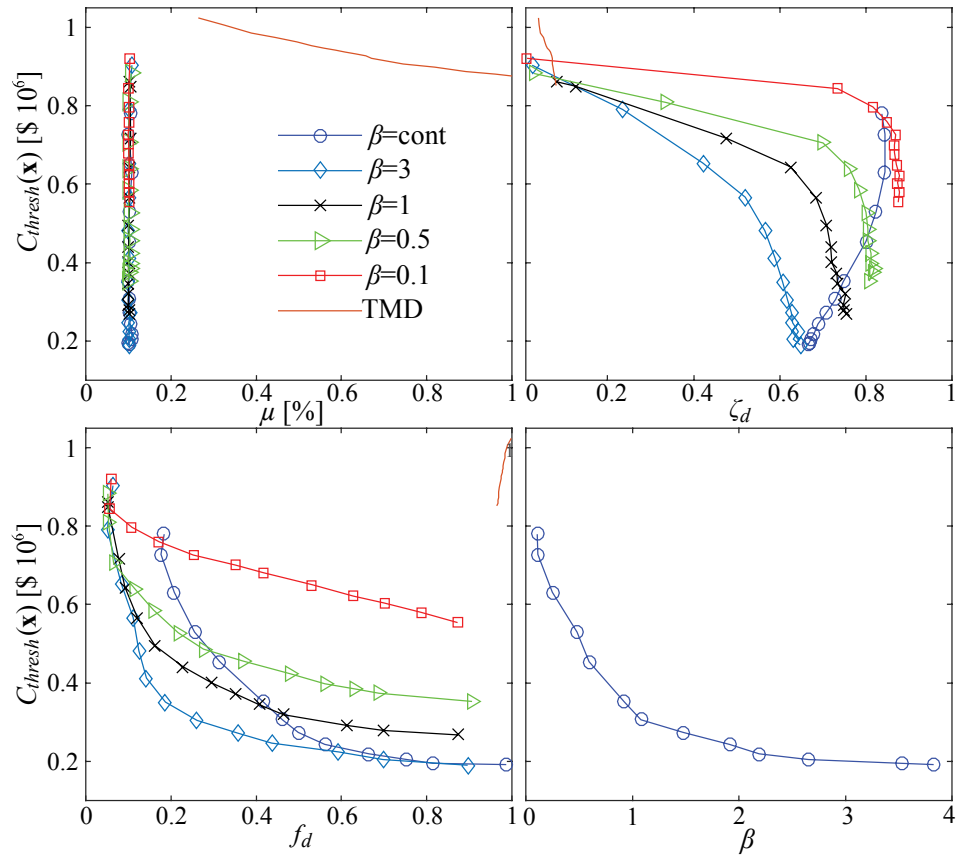
Ruiz R, Taflanidis AA, **Giaralis A,** Lopez-Garcia D. (2018). Risk-informed optimization of the tuned mass-damper-inerter (TMDI) for the seismic protection of multi-storey building structures**.** *Engineering Structures,* **177**: 836-850.

Figure 7. Optimal values for $\mu$, $\zeta_d$, $f_d$ and $\beta$ along the Pareto front [design variables are plotted with respect to the corresponding value of $C_{thresh}(\mathbf{x})$] for $i_d$=21 and $i_b$=18 TMDI configuration. Optimal TMD variables also shown.
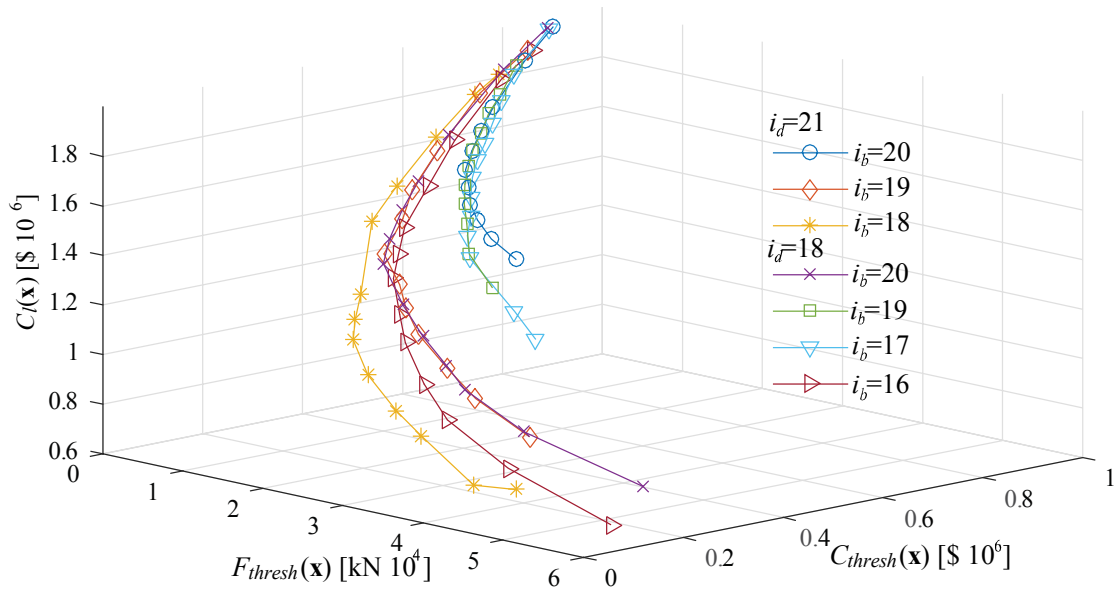


Figure 8. Pareto front in the three-objective space for all examined TMDI topological configurations

Ruiz R, Taflanidis AA, **Giaralis A,** Lopez-Garcia D. (2018). Risk-informed optimization of the tuned mass-damper-inerter (TMDI) for the seismic protection of multi-storey building structures**.** *Engineering Structures,* **177**: 836-850.
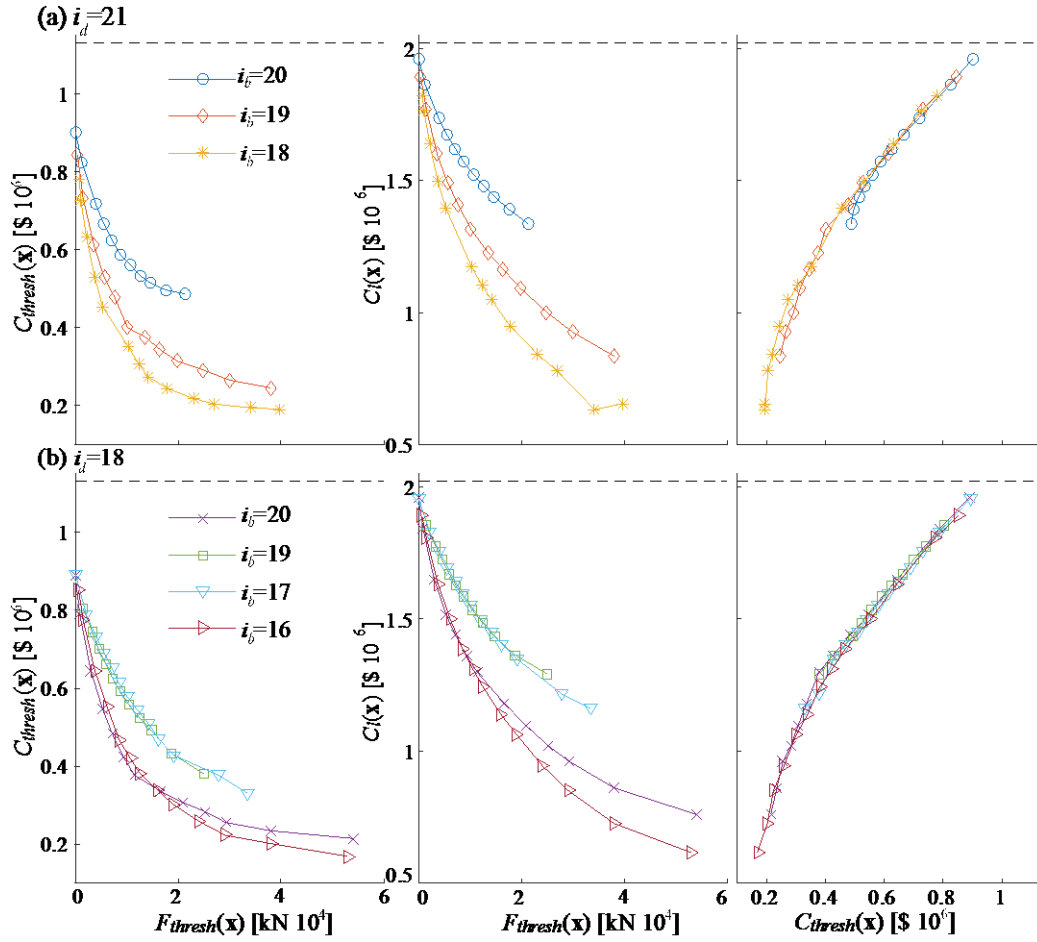
Figure 9. Projection of the Pareto front along pair of objectives for all examined TMDI configurations. Dashed lines correspond to the performance of the structure without the TMDI. Top row corresponds to $i_d$=21 and bottom to $i_d$=18.

## 5.4 Results and discussion for variant design problem

The variant design formulation considers only two objectives $C_l(\mathbf{x})$ and $C_{thresh}(\mathbf{x})$ but the upfront cost in this case is updated to incorporate $F_{thresh}(\mathbf{x})$: $C_i(\mathbf{x})=b_c m+b_b F_{thresh}(\mathbf{x})$. Value of $b_c$ is taken equal to 2500 \$/ton whereas for $b_b$ a parametric investigation is performed considering different values in range [10-100] \$/kN, Note that relationship between upfront cost and reference force demand for other protective devices that exhibit dependence of their implementation cost to such a quantity (reference force demand/capacity) is typically nonlinear [35], with increase in devices capacity coming at proportionally smaller increase of upfront cost. Since no such insight is available for TMDIs implementations this relationship is taken here to be linear. As stressed earlier, this variant design problem is simply investigated to reveal generic patterns. A better understanding of the relationship between $C_i(\mathbf{x})$ and $F_{thresh}(\mathbf{x})$ is warranted for a comprehensive assessment.

Ruiz R, Taflanidis AA, **Giaralis A,** Lopez-Garcia D. (2018). Risk-informed optimization of the tuned mass-damper-inerter (TMDI) for the seismic protection of multi-storey building structures**.** *Engineering Structures,* **177**: 836-850.

Results are only reported for the $i_d$=21 case but for all three possible TMDI topological configurations examined earlier. Also only $\beta$=cont implementation is examined. Trends for all other implementations, including the topological configurations with $i_d$=18, are similar. Figure 12 shows the bi-objective Pareto front and Figures 13-14 the optimal design variables for $i_b$=21 and $i_b$=19 implementations, respectively, in all cases for different $b_b$ values (curves in the plots). Results for the TMDI demonstrate different characteristics than the TMD case, with value of $b_c$ significantly impacting the spread of the Pareto front; for smaller $b_c$ values (i.e. cheaper device implementation) the spread of the front is greatly reduced. This should be attributed to the greater vibration suppression efficiency afforded by the TMDI as also pointed out in previous section. This results in a simultaneous reduction of both the repair cost threshold and the life-cycle cost unless the $F_{thresh}(\mathbf{x})$ value is high enough to increase the latter. Consequently, the part of the Pareto front corresponding to higher $C_{thresh}(\mathbf{x})$ values does not exist for small $b_c$ values; configurations corresponding to larger $C_{thresh}(\mathbf{x})$ values also correspond to large $C_l(\mathbf{x})$ and so are not Pareto optimal. Further, all Pareto front exhibit significant sensitivity which, as pointed out in the previous section, should be carefully examined when selecting the final design configuration (small improvements in one objective come at large compromise of the other).

For all $b_c$ values, the TMDI performance is still superior than the TMD since Pareto front is to the left of the one corresponding to the TMD. A large number of configurations along the identified front leads to higher total cost than the unprotected structure, but at the same time they contribute to significant $C_{thresh}(\mathbf{x})$ reduction. These configurations may be still considered as favorable when decisions are made utilizing risk aversion principles, in other words when focus is only on the mean expected direct losses.

With respect to the identified optimal design configurations, the major difference with the trends reported in the previous section comes from $\mu$: in this case some variation is exhibited along the Pareto front, with most of the Pareto optimal solutions concentrated still on the boundary corresponding to small values for $\mu$. This is an important outcome, showing that larger masses may be indeed beneficial when the total cost of the TMDI is comprehensively evaluated.

Ruiz R, Taflanidis AA, **Giaralis A,** Lopez-Garcia D. (2018). Risk-informed optimization of the tuned mass-damper-inerter (TMDI) for the seismic protection of multi-storey building structures**.** *Engineering Structures,* **177**: 836-850.
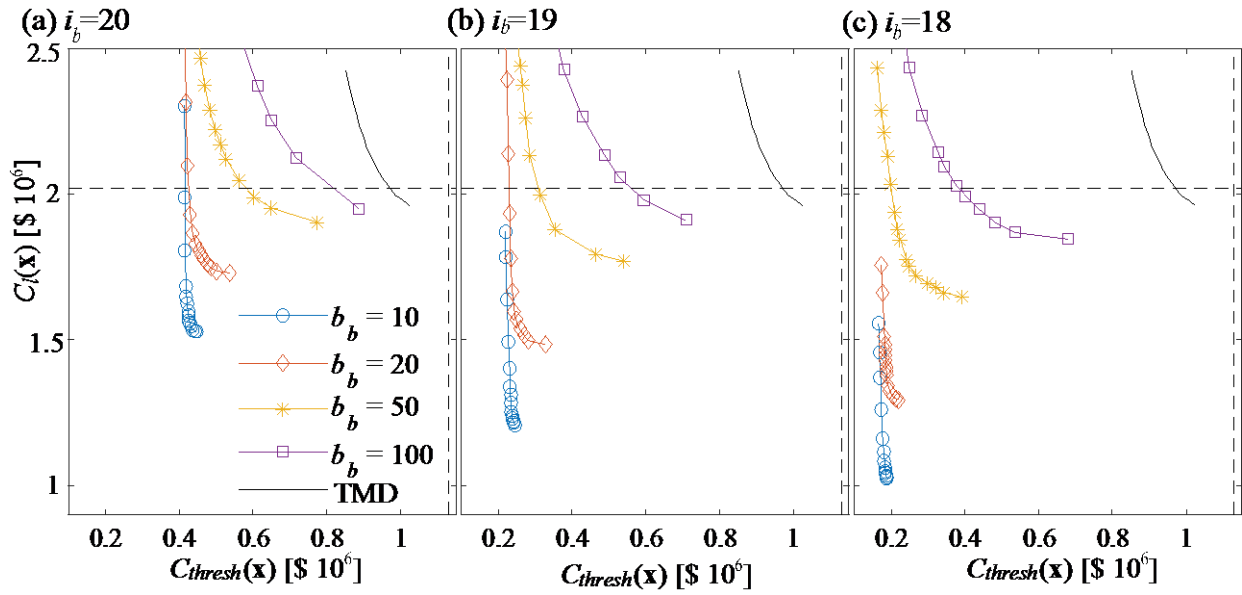
Figure 12. Bi-objective Pareto front for the variant design problem for TMD and TMDI configurations with $i_d$=21. Dashed lines correspond to the performance of the structure without the TMDI.
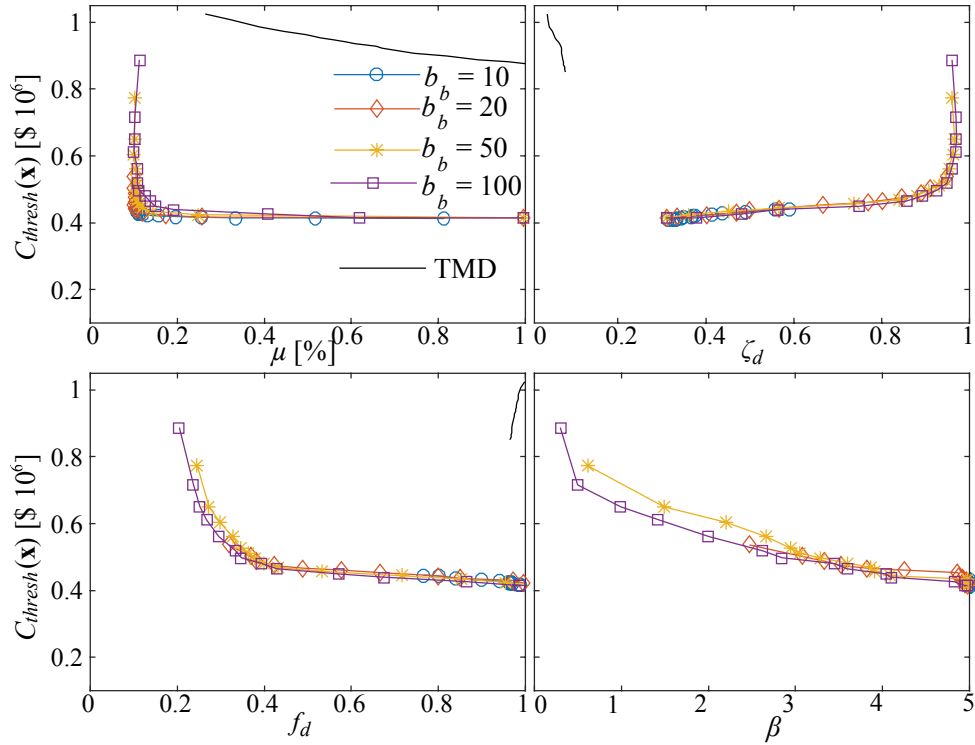


Figure 13. Optimal values for $\mu$, $\zeta_d$, $f_d$ and $\beta$ along the Pareto front for TMD and TMDI configurations corresponding to $i_d$=21 and $i_b$=20.
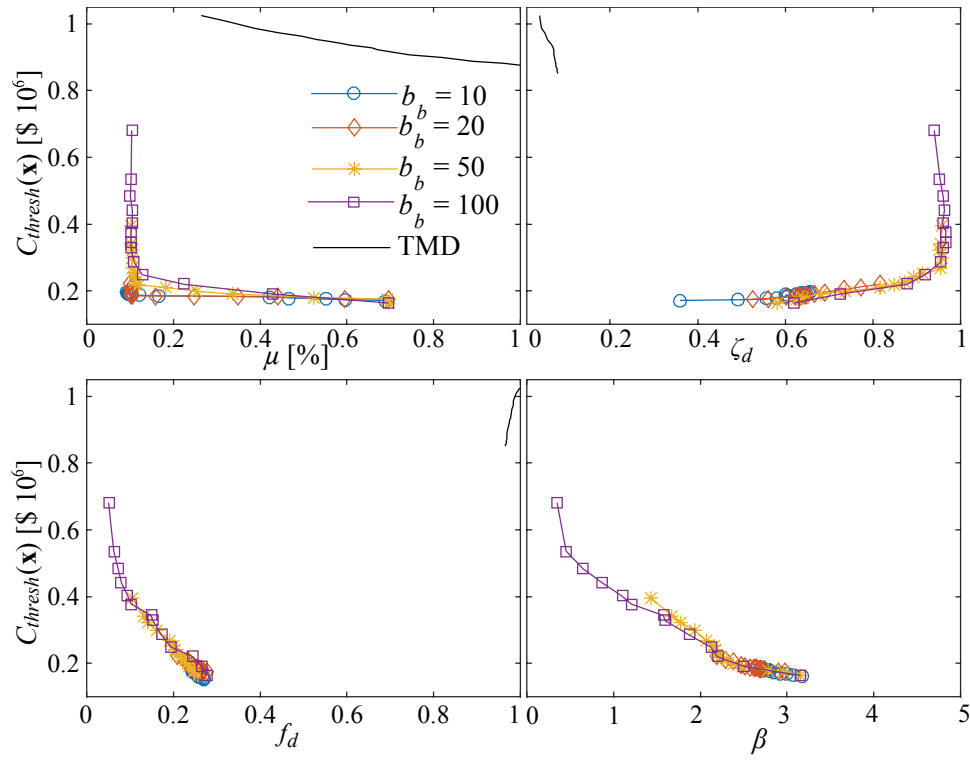
Ruiz R, Taflanidis AA, **Giaralis A,** Lopez-Garcia D. (2018). Risk-informed optimization of the tuned mass-damper-inerter (TMDI) for the seismic protection of multi-storey building structures**.** *Engineering Structures,* **177**: 836-850.

Figure 14. Optimal values for $\mu$, $\zeta_d$, $f_d$ and $\beta$ along the Pareto front for TMD and TMDI configurations corresponding to $i_d$=21 and $i_b$=18.

## 6. Conclusions

The multi-objective design of the tuned-mass-damper-inerter (TMDI) considering life-cycle performance criteria and inerter force was discussed in this paper, focusing on application to seismic protection of multi-story buildings in the region of Chile. Life-cycle performance was evaluated using time-history analysis for describing structural behavior, an assembly-based vulnerability approach for quantifying earthquake losses, and characterization of the earthquake hazard through stochastic ground motion modeling. Three different criteria were utilized in the design optimization. The first one, representing the direct benefits from the TMDI implementation, is the life-cycle cost of the system, composed of the device upfront cost and the anticipated seismic losses over the lifetime of the structure. The upfront device cost was primarily related to the TMDI mass. The other two criteria correspond to performance quantities with specific probability of exceedance over the life-cycle of the structure. Specifically, one corresponds to the repair cost, and incorporates risk-aversion attitudes into the design process, whereas the other corresponds to the inerter force, which incorporates practical constraints for the inerter size and the inerter force transmitted to the host structure. A multi-objective optimization was established considering these three objectives while stochastic simulation techniques were used to obtain all risk measures. A Kriging metamodeling approach was adopted for

Ruiz R, Taflanidis AA, **Giaralis A,** Lopez-Garcia D. (2018). Risk-informed optimization of the tuned mass-damper-inerter (TMDI) for the seismic protection of multi-storey building structures**.** *Engineering Structures,* **177**: 836-850.

facilitating an efficient numerical optimization. In the case study a variant of the design problem was examined, combining the first and third performance objectives, by relating the TMDI implementation upfront cost to both the device mass as well as the reference inerter force.

A case study was presented employing a specific 21-story building located in Santiago, Chile. Seven different topological configurations were examined with TMDI mass attached at the top floor and inerter connecting that mass to the floor either one, two or three stories above or below. The results show that the proposed design framework facilitates a clear demonstration of the benefits of the TMDI, especially when compared to the TMD. The mass-amplification effect facilitated by the TMDI inertance allowed the TMDI to accomplish a simultaneous reduction of both the life-cycle cost and the repair cost along the Pareto front. This comes, though, at the expense of increased inerter forces that need to be transferred by the TMDI to the supporting structure. The developed multi-objective design approach facilitates, nevertheless, a comprehensive evaluation of performance trade-offs. Results also showed that lower inertance values reduce the extent of the Pareto front, and therefore of the dominant designs available for the stakeholder to make the final decision, stressing the importance of technological advances that can produce devices that can accommodate higher inertance values. Connecting the inerter to lower floor also provides considerable benefits across all examined performance criteria and so should be preferred if such a configuration is feasible considering architectural constraints. Incorporation of a cost-component related to the inerter-force demand demonstrated the need for detailed evaluation of the upfront cost related to the inerter implementation; parametric investigation for this cost demonstrated drastically different behavior. For the application examined it was also shown that risk aversion principles can play an important role in the selection of the final design configuration, as multiple members in the Pareto front correspond to increase of the overall cost (compared to the unprotected structure), though, with a simultaneous significant improvement (reduction) of the consequences related to a design level earthquake scenario (infrequent seismic events).

Apart from the practical merit of conclusions drawn based on the furnished numerical results associated with a real-life building structure, it is envisaged that the herein considered optimal design and assessment TMDI framework can be readily modified to accommodate current and future alternative inerter-based mass dampers and passive damping device assemblies, and can be used to evaluate their relative cost-effectiveness in mitigating structural seismic risk.

Ruiz R, Taflanidis AA, **Giaralis A,** Lopez-Garcia D. (2018). Risk-informed optimization of the tuned mass-damper-inerter (TMDI) for the seismic protection of multi-storey building structures. *Engineering Structures,* **177**: 836-850.

**References**
[1] Kareem A. The next generation of tuned liquid dampers.  Proc, First World Conference on Structural Control1994. p. 19-28.
[2] Chang CC. Mass dampers and their optimal designs for building vibration control Engineering Structures. 1999;21:454-63.
[3] Tait MJ, Isyumov N, El Damatty AA. Effectiveness of a 2D TLD and its numerical modeling. Journal of Structural Engineering. 2007;133:251-63.
[4] Feng MQ, Mita A. Vibration control of tall buildings using mega subconfiguration. Journal of engineering mechanics. 1995;121:1082-8.
[5] Den Hartog JP. Mechanical Vibrations. New York, NY: McGraw-Hill, Inc.; 1947.
[6] De Angelis M, Perno S, Reggio A. Dynamic response and optimal design of structures with large mass ratio TMD. Earthquake Engineering & Structural Dynamics. 2012;41:41-60.
[7] Hoang N, Fujino Y, Warnitchai P. Optimal tuned mass damper for seismic applications and practical design formulas. Engineering Structures. 2008;30:707-15.
[8] Matta E. Performance of tuned mass dampers against near-field earthquakes. Structural Engineering and Mechanics. 2011;39:621-42.
[9] Reggio A, De Angelis M. Optimal energy- based seismic design of non- conventional Tuned Mass Damper (TMD) implemented via inter- story isolation. Earthquake Engineering & Structural Dynamics. 2015;44:1623-42.
[10] Lavan O. Multi- objective optimal design of tuned mass dampers. Structural Control and Health Monitoring. 2017;24.
[11] Matta E. Lifecycle cost optimization of tuned mass dampers for the seismic improvement of inelastic structures. Earthquake Engineering & Structural Dynamics. 2018;47:714-37.
[12] Ruiz R, Taflanidis AA, Lopez-Garcia, Vetter C. Life-cycle based design of mass dampers for the Chilean region and its application for the evaluation of the effectiveness of tuned liquid dampers with floating roof. Bulletin of Earthquake Engineering. 2015;14:943-70.
[13] Taflanidis AA, Beck JL. Life-cycle cost optimal design of passive dissipative devices. Struct Saf. 2009;31:508-22.
[14] Shin H, Singh MP. Minimum failure cost-based energy dissipation system designs for buildings in three seismic regions Part II: Application to viscous dampers. Engineering Structures. 2014:DOI: 10.1016/j.engstruct.2014.05.012.
[15] Pollini N, Lavan O, Amir O. Towards realistic minimum-cost optimization of viscous fluid dampers for seismic retrofitting. Bulletin of Earthquake Engineering. 2016;14:971-98.
[16] Marian L, Giaralis A. Optimal design of inerter devices combined with TMDs for vibration control of buildings exposed to stochastic seismic excitations.  11th International Conference on Structural Safety and Reliability. New York, US2013. p. 1025-32.
[17] Marian L, Giaralis A. Optimal design of a novel tuned mass-damper-inerter (TMDI) passive vibration control configuration for stochastically support-excited structural systems. Probabilistic Engineering Mechanics. 2014;38:156-64.
[18] Smith MC. Synthesis of mechanical networks: the inerter. Automatic Control, IEEE Transactions on. 2002;47:1648-62.
[19] Watanabe Y, Ikago K, Inoue N, Kida H, Nakaminami S, Tanaka H et al. Full-scale dynamic tests and analytical verification of a force-restricted tuned viscous mass damper.  15th World Conference on Earthquake Engineering. Lisbon, Portugal2012.
[20] Nakamura Y, Fukukita A, Tamura K, Yamazaki I, Matsuoka T, Hiramoto K et al. Seismic response control using electromagnetic inertial mass dampers. Earthquake Engineering & Structural Dynamics. 2014;43:507-27.
[21] Giaralis A, Taflanidis AA. Reliability-based design of tuned mass-damper-inerter (TMDI) equipped multi-storey frame buildings under seismic excitation.  12th International Conference on Applications of Statistics and Probability in Civil Engineering. Vancouver, Canada2015.

Ruiz R, Taflanidis AA, **Giaralis A,** Lopez-Garcia D. (2018). Risk-informed optimization of the tuned mass-damper-inerter (TMDI) for the seismic protection of multi-storey building structures. *Engineering Structures,* **177**: 836-850.

[22] Giaralis A, Taflanidis A. Optimal tuned mass- damper- inerter (TMDI) design for seismically excited MDOF structures with model uncertainties based on reliability criteria. Structural Control and Health Monitoring. 2018;25:e2082. DOI: 10.1002/stc.2082.
[23] Ikago K, Saito K, Inoue N. Seismic control of single-degree-of-freedom structure using tuned viscous mass damper. Earthquake Engineering & Structural Dynamics. 2012;41:453-74.
[24] Lazar IF, Neild SA, Wagg DJ. Using an inerter-based device for structural vibration suppression. Earthquake Engineering & Structural Dynamics. 2013;43:1129-47.
[25] Hwang J-S, Kim J, Kim Y-M. Rotational inertia dampers with toggle bracing for vibration control of a building structure. Engineering Structures. 2007;29:1201-8.
[26] Giaralis A, Marian L. Use of inerter devices for weight reduction of tuned mass-dampers for seismic protection of multi-story building: the Tuned Mass-Damper-Interter (TMDI). SPIE 9799, Active and Passive Smart Structures and Integrated Systems Las Vegas, Nevada2016. p. doi:10.1117/12.2219324.
[27] Pietrosanti D, De Angelis M, Basili M. Optimal design and performance evaluation of systems with Tuned Mass Damper Inerter (TMDI). Earthquake Engineering & Structural Dynamics. 2017.
[28] Giaralis A, Petrini F. Wind-induced vibration mitigation in tall buildings using the tuned mass-damper-inerter. Journal of Structural Engineering. 2017;143:04017127.
[29] Ikago K, Sugimura Y, Saito K, Inoue N. Modal response characteristics of a multiple-degree-of-freedom structure incorporated with tuned viscous mass dampers. Journal of Asian Architecture and Building Engineering. 2012;11:375-82.
[30] Krenk S, Høgsberg J. Tuned resonant mass or inerter-based absorbers: unified calibration with quasi-dynamic flexibility and inertia correction. Proceedings of the Royal Socociety A. 2016;472:20150718.
[31] Wen Y, Chen Z, Hua X. Design and Evaluation of Tuned Inerter-Based Dampers for the Seismic Control of MDOF Structures. Journal of Structural Engineering. 2016;143:04016207.
[32] Zhang SY, Jiang JZ, Neild S. Optimal configurations for a linear vibration suppression device in a multi- storey building. Structural Control and Health Monitoring. 2017;24.
[33] Takewaki I, Murakami S, Yoshitomi S, Tsuji M. Fundamental mechanism of earthquake response reduction in building structures with inertial dampers. Structural Control and Health Monitoring. 2012;19:590-608.
[34] Boroschek R, Contreras V. Strong ground motion form the 2010 Mw 8.8 Maule Chile earthquake and attenuation relations for Chilean subduction zone interface earthquakes. International Symposium on Engineering Lessons Learned from the 2011 Great East Japan earthquake. Tokyo, Japan2012.
[35] Gidaris I, Taflanidis AA, Mavroeidis GP. Multiobjective design of supplemental seismic protective devices utilizing lifecycle performance criteria. Journal of Structural Engineerinf, ASCE. 2018;144:04017225.
[36] Cha EJ, Ellingwood BR. Seismic risk mitigation of building structures: The role of risk aversion. Struct Saf. 2014;40:11-9.
[37] Haukaas T. Unified reliability and design optimization for earthquake engineering. Probabilistic Engineering Mechanics. 2008;23:471-81.
[38] Massone LM, Bonelli P, Lagos R, Lüders C, Moehle J, Wallace JW. Seismic design and construction practices for RC structural wall buildings. Earthquake Spectra. 2012;28:S245-S56.
[39] Marian L, Giaralis A. The tuned mass-damper-inerter for harmonic vibrations suppression, attached mass reduction, and energy harvesting. Smart Structures and Systems. 2017.
[40] Gonzalez- Buelga A, Lazar IF, Jiang JZ, Neild SA, Inman DJ. Assessing the effect of nonlinearities on the performance of a tuned inerter damper. Structural Control and Health Monitoring. 2016;24:e1879.
[41] Goulet CA, Haselton CB, Mitrani-Reiser J, Beck JL, Deierlein G, Porter KA et al. Evaluation of the seismic performance of code-conforming reinforced-concrete frame building-From seismic hazard to collapse safety and economic losses. Earthquake Engineering and Structural Dynamics. 2007;36:1973-97.
[42] Porter KA, Kiremidjian AS, LeGrue JS. Assembly-based vulnerability of buildings and its use in performance evaluation. Earthquake Spectra. 2001;18:291-312.
[43] Gidaris I, Taflanidis AA. Performance assessment and optimization of fluid viscous dampers through life-cycle cost criteria and comparison to alternative design approaches. Bulletin of Earthquake Engineering. 2015;13:1003-28.
[44] Spall JC. Introduction to stochastic search and optimization. New York: Wiley-Interscience; 2003.

Ruiz R, Taflanidis AA, **Giaralis A,** Lopez-Garcia D. (2018). Risk-informed optimization of the tuned mass-damper-inerter (TMDI) for the seismic protection of multi-storey building structures. *Engineering Structures,* **177**: 836-850.

[45] Coello CAC, Van Veldhuizen DA, Lamont GB. Evolutionary algorithms for solving multi-objective problems: Springer; 2002.
[46] Zemp R, de la Llera JC, Roschke P. Tall building vibration control using a TM-MR damper assembly: Experimental results and implementation. Earthquake Engineering & Structural Dynamics. 2011;40:257-71.
[47] Leyton F, Ruiz S, Sepulveda SA. Preliminary re-evaluation of probabilistic seismic hazard assessment in Chile: from Arica to Taitao Peninsula. Advances in Geosciences. 2009;22:147-53.
[48] Ordaz MG, Cardona O-D, Salgado-GÃ¡lvez MA, Bernal-Granados GA, Singh SK, Zuloaga-Romero D. Probabilistic seismic hazard assessment at global level. International Journal of Disaster Risk Reduction. 2014;10:419-27.
[49] Lamprou A, Jia G, Taflanidis AA. Life-cycle seismic loss estimation and global sensitivity analysis based on stochastic ground motion modeling. Engineering Structures. 2013;54:192–206.
[50] Franchin P, Petrini F, Mollaioli F. Improved risk- targeted performance- based seismic design of reinforced concrete frame structures. Earthquake Engineering & Structural Dynamics. 2018;47:49-67.
[51] Tse KT, Kwok KCS, Tamura Y. Performance and cost evaluation of a smart tuned mass damper for suppressing wind-induced lateral-torsional motion of tall structures. Journal of Structural Engineering. 2012;138:514-25.
[52] Kohavi R. A study of cross-validation and bootstrap for accuracy estimation and model selection. International Joint Conference on Artificial Intelligence1995. p. 1137-45.
[53] Saitua F, Lopez-Garcia D, Taflanidis AA. Cost based design and performance of supplemental viscous dampers attached to non-consecutive floors.  16th European Conference in Earthquake Engineering. Thessaloniki, Greece 2018.
[54] Vetter C, Taflanidis AA, Mavroeidis GP. Tuning of stochastic ground motion models for compatibility with ground motion prediction equations. Earthquake Engineering and Structural Dynamics. 2016;45:893-912.
[55] Jalayer F, Beck JL. Effects of two alternative representations of ground-motion uncertainty in probabilistic seismic demand assessment of structures. Earthquake Engineering and Structural Dynamics. 2008;37:61-79.

## Appendix A: Details for risk characterization and estimation

This Appendix offers some further details on the risk characterization and estimation quantified through the framework overviewed in Figure 2.  Structural behavior is evaluated through response history analysis and a site-specific stochastic ground motion model is adopted to represent seismic input action in terms of acceleration time-histories within a Monte Carlo simulation-based context. In particular, acceleration time-histories are generated by modulating a white noise sequence through parametric functions that account for the frequency and time-domain characteristics of the ground motion excitation. The parameters of these functions are related to seismological parameters, namely the moment magnitude $M$ and the rupture distance $r_{rup}$, through predictive relationships. For the case study discussed in this paper these predictive relationships are tuned [54] to provide a compatibility to the regional (Chilean) hazard by establishing a match to regional ground motion prediction equations [34]. Once the stochastic ground motion model is defined, the adoption of probability distributions for the seismological parameters facilitates the desired probabilistic description of the seismic hazard [55]. Within this setting, each consequence measure $h_r(.)$, used in Eq. (5) to describe seismic risk,  is related to (i) the earthquake performance/losses that can be calculated based on the estimated response of the structure (performance given that some seismic event has occurred), as well as to (ii)

Ruiz R, Taflanidis AA, **Giaralis A,** Lopez-Garcia D. (2018). Risk-informed optimization of the tuned mass-damper-inerter (TMDI) for the seismic protection of multi-storey building structures**.** *Engineering Structures,* **177**: 836-850.

assumptions made about the rate of occurrence of earthquakes (incorporation of the probability of seismic events occurring).

A particularly important consequence measure for the life-cycle cost evaluation is the present value of expected future seismic losses in Eq. (6) which is related to the repair cost given the occurrence of an earthquake event $C_r(\boldsymbol{\theta},\mathbf{x})$. In the adopted approach this cost $C_r(\boldsymbol{\theta},\mathbf{x})$ is estimated through an assembly-based vulnerability approach [42]. According to the latter approach, the components of the structure are grouped into damageable assemblies and different damage states are designated to each assembly. A fragility function (quantifying the probability that a component has reached or exceeded its damage state) and a repair cost estimates are established for each damage state. The former is conditional on some engineering demand parameter (*EDP*), which is related to some peak structural response quantity of interest (e.g. peak interstory drift, peak floor acceleration, etc.). Combination of the fragility and cost information provides then $C_r(\boldsymbol{\theta},\mathbf{x})$.

Seismic risk, ultimately given by Eq. (5), is estimated through stochastic simulation as in Eq. (12) . The estimation of cost threshold $C_{thresh}(\mathbf{x})$ (or $F_{thresh}(\mathbf{x})$ for the inerter force) corresponds to an inverse problem (identify threshold corresponding to a specific probability) which is efficiently solved as follows. First, the required value for $P[C_r > C_{thresh}(\mathbf{x})\,|\,\mathbf{x}, \text{seismic event}]$ (or $P[F_i > F_{thresh}(\mathbf{x})\,|\,\mathbf{x}, \text{seismic event}]$ ) is calculated so that probability $P[C_r > C_{thresh}(\mathbf{x})\,|\,\mathbf{x}, t_{life}]$ is equal to $p_{or}$ (or $p_{oi}$ for $P[F_i > F_{thresh}(\mathbf{x})\,|\,\mathbf{x}, t_{life}]$) though Eq. (7) as

$$P_{target}[C_r > C_{thresh}(\mathbf{x})\,|\,\mathbf{x}, \text{seismic event}] = \ln\left(1 - p_{or}\right)\big/\left(-v t_{life}\right) . \qquad (13)$$

Then, the available samples for the corresponding risk consequence measure $I_C(\boldsymbol{\theta},\mathbf{x})$ (or $I_i(\boldsymbol{\theta},\mathbf{x})$ for the interter force) from the stochastic simulation setting are put in descending order. Lastly, the $N_{target}$ value of $C_r(\boldsymbol{\theta}^j,\mathbf{x})$ (when samples are ordered) that satisfies the condition

$$\frac{1}{N}\sum_{j=1}^{N_{target}} \frac{p(\boldsymbol{\theta}^j)}{q(\boldsymbol{\theta}^j)} = P_{tar}[C_r > C_{thresh}(\mathbf{x})\,|\,\mathbf{x}, \text{seismic event}] \qquad (14)$$

is $C_{thresh}(\mathbf{x})$.